Journal of Natural Resources and Environmental Management
https://dx.doi.org/10.29244/jpsl.16.3.380

RESEARCH ARTICLE

OPEN ACCESS

Check for updates

GIS Modelling for Assessing Flood Risk: A Case Study in Sumbermanjing Wetan District, Malang Regency, Indonesia

Listyo Yudha Irawan[a], Muhammad Nurul Huda[a], Irfan Helmi Pradana[a], Mohammad Tahir B Mapa[b]

[a] Department of Geography, Faculty of Social Sciences, Universitas Negeri Malang, Malang, 65145, Indonesia
[b] Geography Programme, Faculty of Social Sciences and Humanities, Universiti Malaysia Sabah, Sabah, 88400, Malaysia

Article History
Received
09 September 2025
Revised 13 April 2026
Accepted 14 April 2026

Keywords
disaster management,
flood, risk assessment,
spatial analysis,

ABSTRACT

Flood hazard in rural Indonesia is a constant issue, yet detailed risk assessments at the sub-district level are still lacking. This study creates a GIS-based multi-index framework to assess flood risk in Sumbermanjing Wetan District, Malang Regency. It combines hazard, vulnerability, and capacity dimensions using spatial and socioeconomic data. The hazard assessment looks at land system characteristics, average rainfall over the past decade, land cover, and topographic features from a 12-meter resolution ALOS PALSAR DEM. Vulnerability and capacity are based on demographic and institutional indicators. We normalized variables and combined them into composite indices, resulting in a flood risk map for the entire district. Low hazard conditions cover 62.00% of the study area. Most of the vulnerability is moderate (68.48%), while 28.24% of the area is classified as high vulnerability. Medium capacity levels account for 64.30%, but they are unevenly spread throughout the region. Additionally, 32.11% of the district falls into the high-risk category. The highest-risk zones are found in four villages: Argotirto, Harjokuncaran, Tegalrejo, and Sitiarjo. The results indicate that socioeconomic factors and limited options for adaptation, rather than the severity of physical hazards, drive this risk. Therefore, efforts to reduce flooding in rural areas should focus on building social resilience rather than solely relying on physical infrastructure. Immediate steps in these four villages should include improving healthcare access, increasing emergency preparedness, and creating alternative income sources. Even though this study does not validate hydrodynamic modeling, the framework provides practical and clear guidance for prioritizing disaster management in data-limited areas.

Introduction

Flood exposure around the world is rising due to unpredictable rainfall from global climate changes [1–2]. Southeast Asian nations, particularly Indonesia, are worried about the hydro-meteorological risks linked to extreme rainfall and rapid land use changes [3–5]. Floods are the most common disaster in this region. They destroy farmland, damage housing, and seriously disrupt community health [6–9]. From 2014 to 2019, Indonesian national records documented over 1,500 different flood events. This high number highlights how constant the threat has become [10].

Extreme rainfall is only one trigger. Catchment shrinkage, heavy channel sedimentation and physical river narrowing strongly control floodwater propagation [11–13]. Also, heavy deforestation and urban growth reduce the infiltration capacity of soils. Such land alterations increase surface runoff, forcing drainage systems to go beyond their maximum limits [14]. Modern risk assessments are therefore no longer solely based on rainfall thresholds. Currently, researchers integrate hazard, exposure and vulnerability into multi-dimensional assessments [15,16]. These assessments are facilitated by Geographic Information System (GIS) techniques, which offer powerful spatial tools for multi-criteria analysis across different administrative boundaries [17–19].

Corresponding Author: Listyo Yudha Irawan irawanlistyo.fis@um.ac.id Department of Geography, Faculty of Social Sciences, Universitas Negeri Malang, Malang, 65145, Indonesia.

Flood risk mapping methods are constantly evolving. Recent studies have used remote sensing, hydrodynamic simulations, and uncertainty models to generate high-precision spatial data [20–23]. But there is a big bottleneck. Developing countries rarely have computational infrastructure, high-resolution datasets, or technical expertise to run these complex models [24]. Therefore, local governments still depend greatly on simple index-based assessments. However, researchers frequently use simpler models without verifying their structural assumptions. Spatial flood research in Indonesia is highly biased toward urban engineering solutions. Rural areas are still mostly uncharted. Existing literature rarely considers rural hazard, vulnerability and adaptive capacity as equally important variables [25,26]. This is a huge gap; we need urgent, realistic, context-specific risk-assessment designs for data-poor rural areas.

Sumbermanjing Wetan District in Malang Regency highlights a clear analytical gap. Over the past ten years, severe floods have repeatedly destroyed local livelihoods and submerged residential areas [27]. This study develops a GIS multi-index framework at the village level to tackle this problem. Unlike earlier research that primarily focused on detecting physical hazards, we consider hazard, vulnerability, and adaptive capacity to be equally important factors. By combining capacity metrics based on the Sendai Framework for Disaster Risk Reduction, we create a detailed risk map for rural areas. We demonstrate that simple, low-data methods can still yield useful spatial information. Three main questions guide this research: (1) What is the spatial distribution of flood hazard, vulnerability, and adaptive capacity across Sumbermanjing Wetan? (2) How do these three indices interact to form the final risk map? (3) Which specific villages need immediate attention for mitigation?

Materials and Methods

Study Area

Sumbermanjing Wetan District is located in the southern part of Malang Regency, East Java. It borders the Indian Ocean. The area's physical landscape is dynamic. The geomorphological features include lowland plains, rolling hills, and narrow coastal strips. A dense network of rivers runs from north to south and drains into the southern coast. This layout quickly traps surface runoff during heavy rain or storms. Data from the last ten years shows a trend of severe flooding. These floods often destroy farms, cut off neighborhoods, and disrupt local businesses. Poor planning makes the situation worse [27]. Residents continue to build homes and grow crops near active river channels or in low-lying areas that struggle with drainage. The Panguluran River is a major source of flooding. Heavy rainfall often exceeds the river's channel capacity, causing it to overflow into nearby villages. At the same time, aggressive farmland expansion and rapid population growth clear important forests and shrublands. This significant change in land use reduces the soil's ability to absorb water. It also accelerates runoff and increases downstream flood volume.

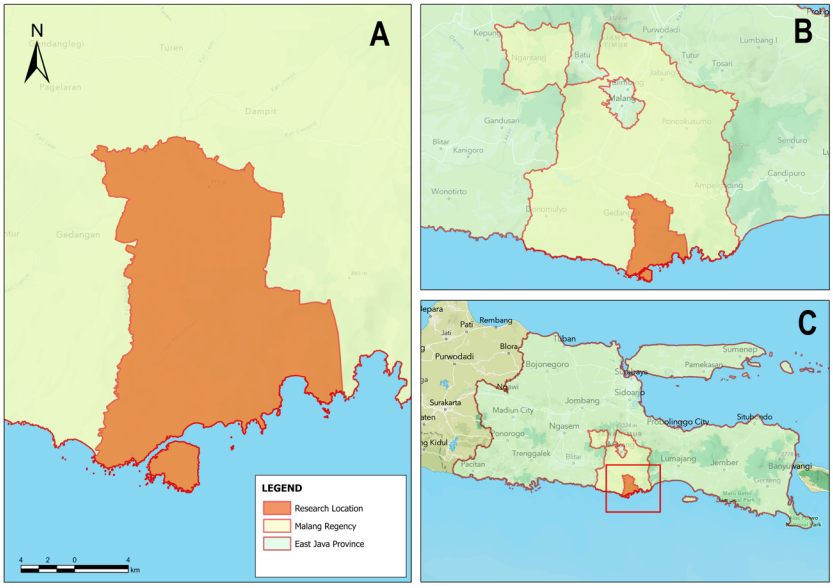

Figure 1. Geographical location of Sumbermanjing Wetan District, Malang Regency, East Java. The main map displays the internal boundaries of administrative villages. Inset maps offer the larger regional context. The southern boundary of the district directly borders the Indian Ocean.

Materials

This study gets its physical and environmental variables from secondary data. We carefully chose these datasets because of their known impact on local hydrological and geomorphological flood processes. The initial spatial inputs included both raster and vector formats. This variety in formats required preprocessing before any GIS work. We adjusted and resampled all layers to ensure a consistent spatial resolution and projection system, ensuring geometric compatibility. Table 1 lists the complete set of dataset types, spatial parameters, and the agencies that published them.

Table 1. Secondary spatial datasets, model parameters, and institutional sources are used in the flood risk assessment. It relies on five main inputs. These are land systems, rainfall records, land use maps, ALOS PALSAR DEM, and administrative boundaries. These layers directly influence the local hydrological and geomorphological hazard processes.

Data	Parameters
Land System	Soil texture, surface drainage, puddle conditions
Rainfall (10-year average)	Annual precipitation
Land Use Map (1:25,000)	Land cover types
DEM (ALOS PALSAR, 12 m)	Elevation, slope classes
Administrative Boundaries	District boundaries

Methods

A descriptive quantitative method organized this research into three indices: hazard, vulnerability, and capacity. Each index was classified as low, medium, or high. The analysis used equal interval classification across all three datasets. This technique was chosen because the initial index values showed fairly uniform distributions. It also maintains interval comparability across indices, following the Natural Agency for Disaster Management's (*Badan Nasional Penanggulangan Bencana*/BNPB) practical guidelines for disaster risk assessment [28]. Before the classification stage, descriptive statistics and histogram plots were used to verify the data. These tests confirmed nearly symmetrical distributions with slight skewness. We also tested quantile and natural breaks algorithms, but rejected both because they disrupted the cross-index comparability needed for this spatial application. In addition, the BNPB General Guidelines recommend simple classification schemes for operational disaster management.

The hazard index construction identified physical factors that directly lead to local floods. We determined variable weights using the Analytic Hierarchy Process (AHP) [29,30]. These weights came from a pairwise comparison matrix. The analytical workflow maintained the consistency ratio below 0.1 during all calculations. Instead of using a generic method, we adjusted the matrix to reflect Sumbermanjing Wetan's specific flood behavior. While this weighting system is clear and consistent, it relies heavily on subjective pairwise judgments. Since the research did not include formal expert input or field calibration, there may be minor biases. Additionally, the study did not perform sensitivity analyses or hydrodynamic validations against actual flood extents.

The vulnerability index combines physical, socioeconomic, and environmental factors to assess the extent to which populations are exposed and the potential losses they may face [31]. The capacity index, on the other hand, used different measures. It examined the availability of health facilities, the number of medical staff, community readiness for disasters, and local institutional strength. These factors indicate how well local residents can handle and recover from the impacts of floods [32]. The raw data for both indices were obtained directly from the Statistics Indonesia (*Badan Pusat Statistik*/BPS) and BNPB archives. This data was in various formats, mixing quantitative tables with qualitative disaster reports. The vulnerability variables were grouped into socioeconomic, physical, and environmental categories. Capacity parameters were categorized into health services, public facilities, and institutional frameworks. Table 2 provides a detailed breakdown of the parameters used for this localized flood risk index.

Table 2. Index-construction framework for spatial risk assessment. The table lists the hazard, vulnerability, and capacity components. Hazard variables rely only on physical flood triggers. Vulnerability includes specific socioeconomic, physical, and environmental metrics. Capacity focuses on health services, public infrastructure, and institutional readiness. A min-max transformation rescaled all raw variables into a standardized range from 0 to 1 before the final aggregation.

Index	Parameters (Criteria)	Variable
Hazard	Physical	Land system (soil texture, surface drainage, and conditions for the existence of ponds)
		Hydrology (average rainfall)
		Cover land (type land use)
		Topography (slope)
Vulnerability	Socio-Economic	Population density (persons/km^2)
	Physical	Sex ratio (%)
		Productive land area (Km^2)
	Environment	House (units)
		Public facilities (unit)
		Forest area (ha)
		Shrub area (ha)
Capacity	Health	Health workers
		Health facilities
	Public	Disaster anticipation
	Institutions and organizations	Obtaining assistance
		Disaster socialization

Table 3 shows the pairwise comparison matrix for the chosen hazard parameters. This matrix shows their relative spatial weights. The evaluation included four variables: land system, rainfall, land use, and slope. These geomorphological and hydrological factors greatly affect local flood mechanisms. Previous research supports their inclusion. Limited local data also influenced the selection process. The final list of variables represents a careful balance between analytical detail and what was practically available. The matrix scores indicate how much each parameter influences flood generation. We used standard AHP scaling for this evaluation [18,30]. Previous studies and local flood knowledge informed our weight assignments. We did not conduct a structured expert elicitation. This method maintains transparency but also introduces unavoidable subjectivity in judgment. Matrix normalization produced distinct parameter weights (Table 4). The land system received the highest weight at 0.576. Rainfall followed with 0.240, then land use at 0.112, and slope at 0.072. Lastly, the Consistency Ratio was calculated at 0.024. This value easily meets the required limit of 0.1. Such a result ensures valid internal consistency for the pairwise judgments [18,30].

Table 3. AHP pairwise comparison matrix for the four hazard parameters. The parameters are land system, rainfall, land use, and slope. The valuation uses the standard AHP scale. Cell entries denote the relative importance between parameter pairs. The matrix prioritizes the land system as the leading physical control over local flood susceptibility.

Variable	Land System	Rainfall	Land Use	Slope
Land System	1	3	5	7
Rainfall	0.33	1	3	3
Land Use	0.2	0.33	1	2
Slope	0.142	0.33	0.5	1

Table 4. Normalized decision matrix showing relative contributions of hazard parameters to flood occurrence in Sumbermanjing Wetan District. Values are normalized column-wise so that the sum equals 1. The last column shows the average weight of each parameter.

Variable	Land System	Rainfall	Land Use	Slope	Average (Weight)
Land System	0.597	0.643	0.526	0.538	0.576
Rainfall	0.199	0.214	0.316	0.231	0.24
Land Use	0.119	0.071	0.105	0.154	0.112

Variable	Land System	Rainfall	Land Use	Slope	Average (Weight)
Slope	0.085	0.071	0.053	0.077	0.072
Total	1	1	1	1	1

A sensitivity analysis was carried out to assess the stability of the hazard index under moderate changes in the AHP-derived weights. Each parameter weight was shifted by ±10% to produce alternative weighting scenarios, and the resulting hazard index values were compared against the baseline. The modified weights applied in each scenario are listed in Table 5.

Table 5. Hazard parameter weights used in the sensitivity analysis for Sumbermanjing Wetan District, Malang Regency, showing original AHP-derived weights and values perturbed by +10% and -10% for land system, rainfall, land use, and slope. These modified weights were applied to test whether moderate variations in expert-based weighting assumptions would alter the spatial classification of flood hazard across the study area.

Parameter	Original Weight	+10% Scenario	-10% Scenario
Land System	0.576	0.634	0.518
Rainfall	0.24	0.264	0.216
Land Use	0.112	0.123	0.101
Slope	0.072	0.079	0.065

Spatial classifications produced under both perturbation scenarios were identical to those of the baseline hazard model, suggesting that the model remains reasonably stable to moderate shifts in parameter weighting. BPS and BNPB archives provided the socioeconomic, physical, and environmental indicators for the vulnerability index. The raw datasets used different measurement units. Inputs included total house counts, forest cover in hectares, sex-ratio percentages, and population density. You cannot directly add these raw metrics together. The workflow then applied min-max normalization. This method rescales every indicator into a dimensionless range of 0 to 1 based on district-level extremes. This mathematical change standardizes all data. It removes unit differences before the final aggregation process. This prevents incorrect composite scores, enabling the composite vulnerability total to be calculated as expressed in Equation 1.

$$VT = 0.5(SEV) + 0.35(PV) + 0.15(EV) \quad (1)$$

Information:

VT = vulnerability total

SEV = socio-economic vulnerability

PV = physical vulnerability

EV = environmental vulnerability

The capacity index measures village-level resilience in accordance with the Sendai Framework for Disaster Risk Reduction 2015 to 2030 [33]. It includes five specific indicators: the number of health workers, the availability of health facilities, disaster preparedness, the accessibility of assistance, and disaster socialization programs. These factors focus on readiness. Health personnel and facilities demonstrate the ability to respond quickly. Anticipation and socialization metrics show how prepared the community is. Assistance accessibility shows the extent of external support. Local healthcare constraints and institutional readiness greatly influence operational disaster response. Additionally, the selection of variables makes sure there is no overlap with the vulnerability index. The capacity assessment looks only at functional readiness and does not repeat socioeconomic metrics. A min-max transformation normalized all indicators into a dimensionless range of 0 to 1 before aggregation. The model gives each indicator an equal weight of 0.2. The Sendai Framework clearly views preparedness and response dimensions as equally important at the local level. This equal weighting approach also addresses the lack of formal expert input. The analysis does not include sensitivity testing. Using uncalibrated equal weights is a recognized limitation of this final capacity index, which is expressed as Equation 2.

$$C = 0.2(HW) + 0.2(HF) + 0.2(DA) + 0.2(OA) + 0.2(DS) \quad (2)$$

Information:

C (capacity) = composite index of village resilience.

HW (health workers) = number of health workers in the village.

HF (health facilities) = availability of local health facilities.

DA (disaster anticipation) = community readiness and anticipatory actions.

OA (obtaining assistance) = ability to seek and receive external support

DS (disaster socialization) = socialization and awareness activities on disasters.

The final flood risk map combines three indices: hazard, vulnerability, and capacity. A spatial overlay process merged these layers into a single output. Disaster risk results from the intensity of hazards and systemic vulnerability. Local adaptive capacity can lower this risk. High scores in hazard and vulnerability increase the chances of losses. On the other hand, strong capacity reduces overall risk. While it doesn't change physical exposure, it does improve the community's response. The model treats hazard and vulnerability as factors that multiply. The capacity index adjusts this product. This framework is based on a few key ideas. First, the main components interact through multiplication instead of addition. Second, normalization ensures that comparisons across variables are fair. Lastly, the model assumes conditions are uniform within each administrative boundary. This is a major simplification. The current scale cannot capture differences within villages. Risk class boundaries follow the criteria in Risk class boundaries follow the criteria in BNPB General Guidelines for Disaster Risk Assessment No. 2 of 2012 [28], applied using Equation 3 as follows:

$$R = \frac{H \times V}{C} \quad (3)$$

Where:

R (risk) = composite index representing the overall flood risk level.

H (hazard) = intensity and probability of flood-triggering factors in the study area.

V (vulnerability) = exposure and sensitivity

C (capacity) = ability of the community and institutions to anticipate, respond, and recover from flood events.

Three main parts guide this research framework: hazard, vulnerability, and capacity. Various raw datasets support these components. Inputs include land system features, rainfall, land use, slope, socioeconomic metrics, and institutional data. Initial preprocessing changed all spatial data into thematic maps. The workflow then performed classification and aggregation to create the composite indices. A spatial overlay combined these three indices. This final step produced the flood risk index. Population density, housing conditions, health facility counts, and disaster preparedness metrics directly shape this final profile. Figure 2 illustrates this exact step-by-step workflow.

This index-based framework acts only as a basic screening tool for spatial prioritization. It does not provide exact flood predictions. Limited data prevented hydrodynamic validation. The study also lacked high-resolution flood-extent mapping. Instead, historical flood records serve only as qualitative reference points for spatial interpretation. Two main factors create uncertainty in the model: subjective parameter weighting and generalization of administrative boundaries. Sensitivity testing of the hazard weights partially tackled the first issue. Additionally, the study does not include formal comparisons with other models. Still, the overall methodology aligns with established GIS multi-index frameworks used in similar data-limited environments.

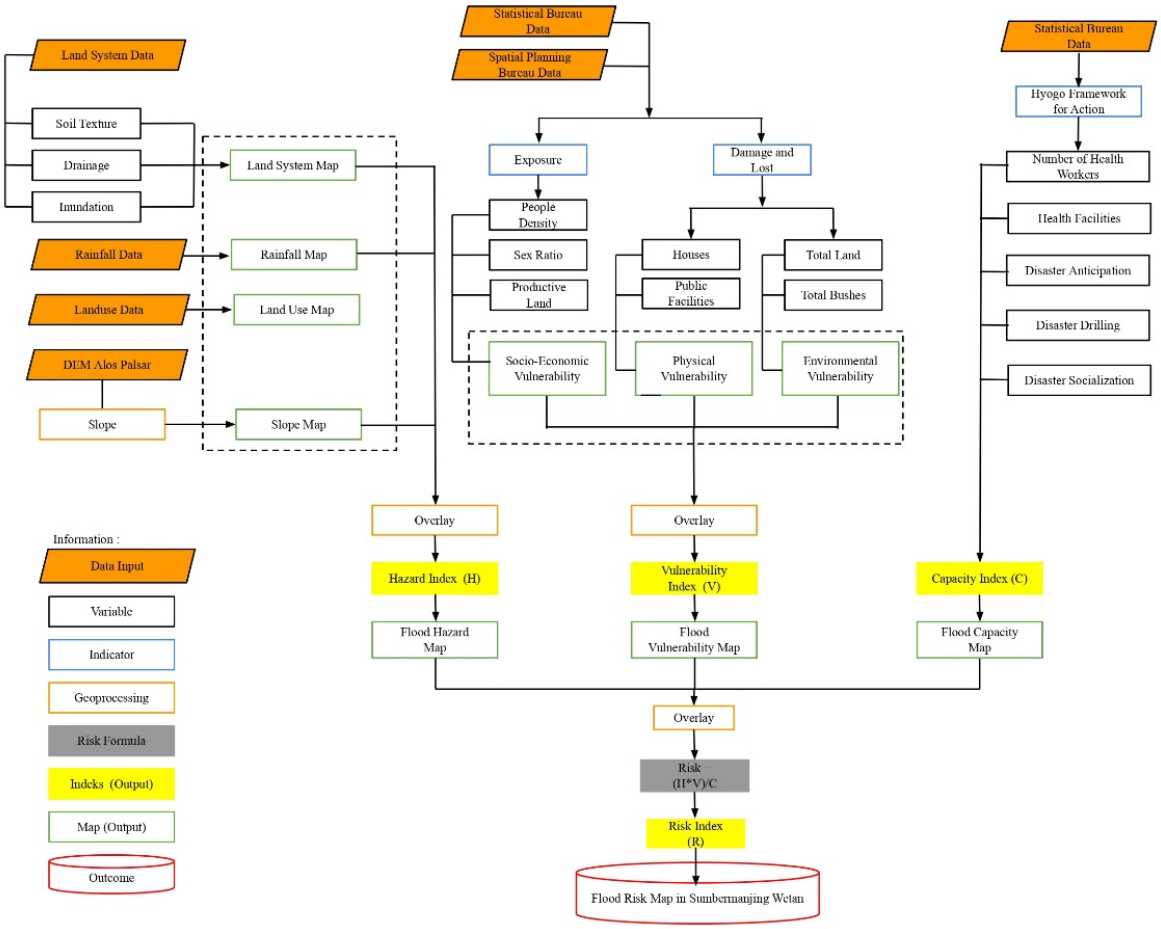

Figure 2. Methodological flowchart for the spatial risk assessment. Raw datasets follow three separate, parallel tracks. The model processes hazard, vulnerability, and capacity components independently. Each track produces a specific composite index. A spatial overlay procedure combines these intermediate outputs. Physical, socioeconomic, and institutional variables are introduced at different stages of the workflow and then come together at the risk classification step.

Results and Discussion

Results

Hazard Index

Table 6 presents the hazard index results. Most of Sumbermanjing Wetan District is in low-hazard zones. This category covers 170.06 km², which is 62.00% of the total area. The medium-hazard class spans 91.83 km², or 33.48%. In contrast, high-hazard areas occupy a small 12.42 km², which is 4.53%. The low-hazard zones are mainly in southern and southeastern coastal villages. Central villages form a medium-hazard band that acts as a transition. High-hazard areas are highly localized. They are found right along active river channels and in land systems with poor drainage. A sensitivity analysis confirmed the model's strength. The workflow altered the baseline AHP weights by ±10% in two different cases. The recalculated indices were then compared to the original baseline. Spatial classifications stayed the same across all setups (Table 6). This indicates stability against moderate weight changes. However, mathematical methods play a part in this stability, rather than just environmental signals. The land system parameter influences the entire AHP formulation. Its heavy, discrete scoring tends to push most of the district into the low-hazard category, even with minor weight shifts. In physical terms, coastal coverage and remaining vegetation reduce surface runoff and improve soil infiltration. These combined factors explain the widespread low-hazard coverage and clarify the firm's spatial outputs. General parameter schemes do not effectively capture localized flood dynamics along smaller channels.

Table 6. Sensitivity analysis outputs for the spatial hazard classification. The table compares the baseline AHP configuration with two structural changes: 10% and 10%. Final spatial boundaries for low, medium, and high hazard classifications remain completely unchanged across all test conditions.

Scenario	Weight Modification	Low Hazard (%)	Medium Hazard (%)	High Hazard (%)
Baseline	Original AHP Weights	62.00	33.48	4.53
Scenario 1	+10% weight perturbation	62.00	33.48	4.53
Scenario 2	-10% weight perturbation	62.00	33.48	4.53

Vulnerability Index

Table 7 shows the vulnerability distribution. Medium-vulnerability zones make up most of Sumbermanjing Wetan District. They cover 188.97 km², which is 68.48% of the total area. High-vulnerability areas cover 77.93 km², representing 28.24% of the total area. In contrast, low-vulnerability zones are small, at 9.03 km² (3.27%). Villages in the north and west show the highest vulnerability. These areas have dense settlements, with residents living close to local administrative and economic centers. This proximity attracts large populations and valuable resources. As a result, flooding poses a serious threat to property and lives in these regions. Central villages have medium vulnerability due to mixed land use. The built environment sits next to farmland. Farmers regularly work the low-lying fields near active river channels. Surface runoff and river overflow frequently flood these agricultural areas. This situation keeps agricultural vulnerability consistently high, regardless of the basic hazard level. Low-vulnerability areas are limited and mostly located in isolated northern villages with very low exposure rates. Ultimately, socioeconomic exposure and land use practices shape the district-wide vulnerability profile. These human factors affect spatial risk more than the raw physical hazard signals.

Capacity Index

The capacity classification identified only two categories for the Sumbermanjing Wetan District. No villages reached the high-capacity level (Table 7, Figure 3c). Most of the study areas consist of medium-capacity zones. This category includes 177.43 km², which is 64.30% of the district. These zones are mainly found in the central and eastern villages. Local health services and institutional readiness are fairly strong in these areas. Low-capacity areas make up the remaining 98.50 km², or 35.70%. This group is primarily made up of isolated rural villages on the district's edge. Disaster response infrastructure is seriously lacking in these outer areas. The absence of high-capacity villages highlights a significant weakness. Local disaster preparedness is still limited by structural issues. This problem affects the entire district, not just specific geographic areas.

Risk Index

Overlaying the three composite indices produces a district-wide flood risk map with three risk classes (Table 7, Figure 4). Low risk areas make up the majority, covering 123.96 km² or 45.19% of the total area. High risk areas extend across 88.07 km² (32.11%), while medium risk covers 62.27 km² (22.70%). Spatially, low risk zones are concentrated in southern coastal villages where higher capacity values coincide with relatively low vulnerability. Medium-risk zones are distributed across the northern part of the district, where hazard, vulnerability, and capacity values interact at intermediate levels.

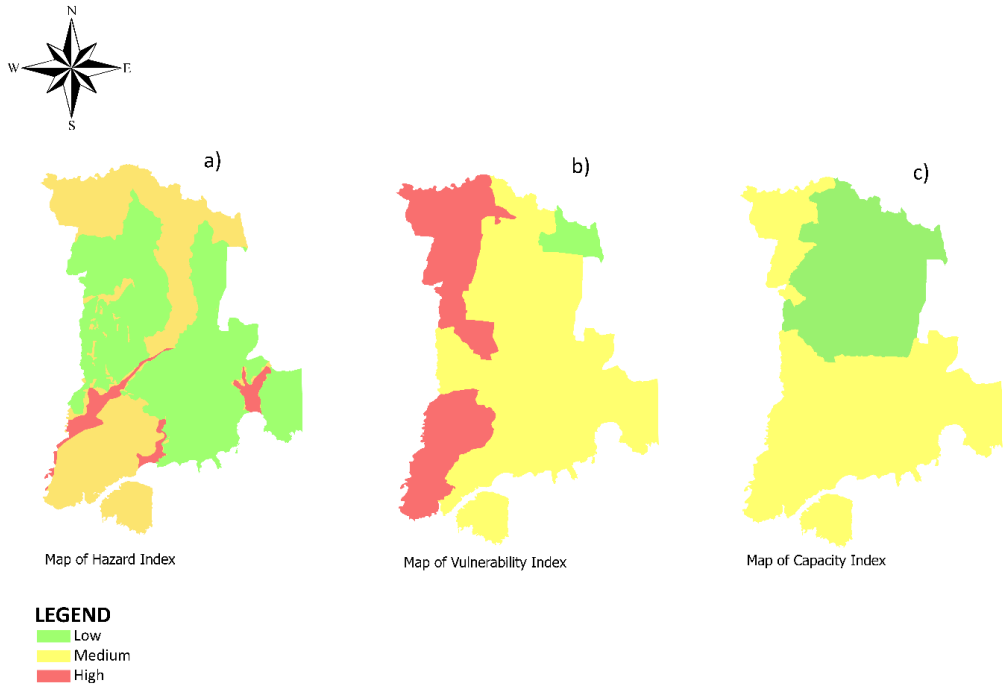

Figure 3. Spatial components of the final flood risk map for Sumbermanjing Wetan District. Panel (a) presents the Hazard Index. AHP weights determine this output based on land systems, rainfall, land use, and slope data. Panel (b) shows the Vulnerability Index. This layer combines different socioeconomic, physical, and environmental factors. Panel (c) illustrates the Capacity Index. The calculation uses health service access, public infrastructure counts, and institutional variables. All indicators were rescaled to a 0–1 range before index aggregation.

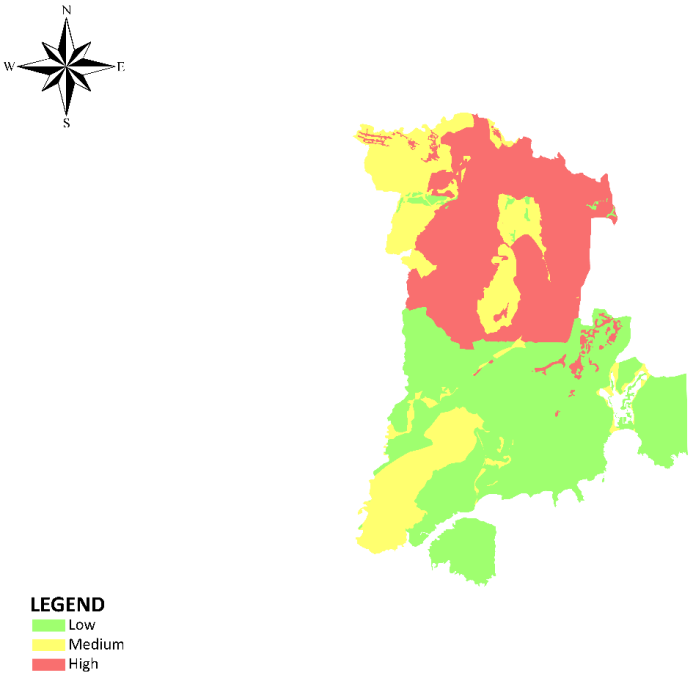

Figure 4. Flood risk map of Sumbermanjing Wetan District, Malang Regency, produced by integrating hazard, vulnerability, and capacity indices following BNPB General Guidelines for Disaster Risk Assessment No. 2 of 2012. High-risk zones account for 32.11% of the district and are concentrated in the northern villages of Argotirto, Harjokuncaran, Tegalrejo, and Sitiarjo.

Table 7. Areal extent and percentage coverage of flood hazard, vulnerability, capacity, and composite risk classes across Sumbermanjing Wetan District, Malang Regency, derived from GIS-based multi-index analysis. Low hazard covers 62.00% of the district, medium vulnerability 68.48%, medium capacity 64.30%, and high risk 32.11%.

Index	Class	Area (km²)	Percentage (%)
Hazard	High	12.42	4.53
	Medium	91.83	33.48
	Low	170.06	62.00
Vulnerability	High	77.93	28.24
	Medium	188.97	68.48
	Low	9.03	3.27
Capacity	Medium	177.43	64.30
	Low	98.50	35.70
Risk	High	88.07	32.11
	Medium	62.27	22.70
	Low	123.96	45.19

Discussion

Overall Flood Hazard Pattern

These recent events suggest the hazard map captures only part of the flood picture in Sumbermanjing Wetan. What occurred in Sitiarjo and Tambakrejo points to flood-prone conditions that static, parameter-based classification does not fully register, and validation against observed inundation extents or hydrodynamic output would be needed to determine how far the model falls short.

Similar mapping issues arise in wider spatial literature. Luu et al. [34] observed this pattern in Quang Nam, Vietnam. They found that unvalidated AHP weights often misrepresent actual hazard intensity. This mistake becomes more pronounced when historical records of flood depth and duration are missing. Nguyen et al. [35] supported this systemic flaw. Standard predictors like rainfall, slope, land use, and drainage are sound in theory. However, their impact varies greatly across different geographical locations. Researchers need to compare these variables with reliable hydrological data to ensure spatial reliability.

The results from Sumbermanjing Wetan highlight this methodological issue. The common low-hazard classification relies on a strict model structure instead of accurately reflecting how the physical landscape responds during heavy rainfall. Despite these challenges, the GIS-AHP integration is still useful. It works well as an initial hazard screening tool in areas with limited data. Recent studies consistently show its value for setting up spatial criteria when data is limited. However, the recent floods in Tambakrejo and Sitiarjo serve as a clear warning. Multi-criteria mapping works as a preliminary spatial filter rather than a final assessment. Future local disaster management must integrate these spatial indices with field records to develop effective interventions at the village level.

Vulnerability Pattern

Spatial vulnerability distributions skew heavily toward the upper thresholds. Medium-vulnerability zones span 68.48% of the district. High-vulnerability coverage reaches 28.24%. Low-vulnerability extents remain statistically marginal at 3.27%. Such extensive spatial exposure guarantees severe economic and physical degradation during inundation. Extreme demographic density directly dictates this vulnerability concentration. Klepu records 894 persons/km². Druju follows closely with 693 persons/km². This precise demographic loading forces massive populations and critical assets directly into active hazard boundaries. Severe healthcare deficits multiply this baseline risk. Institutional records from 2023 confirm only one inpatient health center and six doctors serve over 100,000 residents. This extreme medical ratio systematically fails to absorb post-inundation health crises [29,36].

Absolute agricultural dependency amplifies local exposure. The district operates purely on 11 permanent or semi-permanent market units. *Capsicum frutescens* and *Capsicum annuum* (chili) cultivation entirely dominated the 2023 economic output. Monoculture systems collapse instantly under flood stress. Standing water destroys active crops and serves primary distribution logistics. Lacking alternative economic streams, post-disaster recovery in these settlements strictly stagnates. Existing empirical literature observes identical vulnerabilities in rural Nepal. Subsistence agriculture and absolute resource scarcity physically dictated household-level risk [37]. Systematic geospatial reviews corroborate this multifactorial dynamic. Social,

economic, and environmental indicators constantly function as interdependent networks, never operating in isolation [38].

Asian rural topologies frequently share these exact structural flaws: deficient infrastructure, restricted institutional penetration, and stagnant economic diversification [39]. Sumbermanjing Wetan perfectly mirrors this convergence. Hyper-dense settlements overwhelmed medical logistics, and rigid agricultural reliance directly generate the 28.24% high-vulnerability metric. Consequently, disaster risk reduction requires immediate structural intervention. Regional authorities must drastically expand the active medical workforce and physically upgrade health centers. Furthermore, policymakers must establish alternative economic pathways completely detached from seasonal monoculture cycles [36,37].

Flood Capacity Pattern

Zero villages in Sumbermanjing Wetan achieved high-capacity classifications. Medium-capacity zones constitute 64.30% of the district. Low-capacity areas cover the remaining 35.70%. Demographic ratios expose severe structural deficits. Currently, over 101,000 residents rely on exactly six doctors, 26 nurses, 30 midwives, five pharmacists, and three nutritionists. Physical medical infrastructure remains highly inadequate. The entire district contains only one inpatient health center. Auxiliary facilities include a single clinic, 70 integrated healt posts (*Pos layanan terpadu/posyandu*), and eight pharmacies. Educational infrastructure exhibits identical spatial deficits. Baseline facilities include 121 kindergartens, 51 elementary schools, and 13 junior high schools. Vocational and senior high schools remain statistically negligible. Central administrative villages monopolize these sparse services. Extreme geographic distance severely restricts access for peripheral settlements like Sekarbanyu and Sidoasri [36].

Transportation and communication networks demonstrate extreme spatial asymmetry. All village roads possess paved surfaces ensuring year-round access. Conversely, fixed public transport routes bypass multiple administrative zones entirely. Rural populations consequently depend strictly on irregular transport modes. Communication infrastructure exhibits severe maldistribution. Thirty-two base transceiver stations serve only 15 villages. Harjokuncaran operates seven towers. Tegalrejo possesses zero [36]. This specific communication void paralyses inter-village coordination during inundation events. Emergency response times degrade significantly. Extreme flood events in Thailand demonstrated identical infrastructural constraints [40]. Absolute resource quantities do not guarantee resilience. Effective mitigation strictly requires precise spatial distribution.

International spatial literature corroborates this exact mechanism. Dutch case studies show that knowledge-sharing networks and active community participation significantly improve disaster preparedness. Physical infrastructure alone completely fails to replicate these social buffers [41]. South Korean spatial analysis confirms this dynamic. Local institutional strength and organizational redundancy serve as the primary factors distinguishing resilient from vulnerable urban sectors [42]. Furthermore, physical drainage and transport networks must strictly conform to actual local topography. Statistical benchmarks offer zero operational value during actual floods [43]. Sumbermanjing Wetan fails all these preconditions. Medical services lack functional redundancy. Educational access vanishes at district perimeters. Public transport coverage remains heavily fragmented. Spatial blind spots dominate the communication network. Immediate capacity-building interventions must aggressively redistribute existing services and upgrade peripheral facilities.

Flood Risk Pattern

Spatial risk outputs show that 45.19% of the area is low-risk. High-risk environments account for 32.11% of the district. Medium-risk zones make up the remaining 22.70%. This large high-risk area needs urgent attention. Argotirto, Harjokuncaran, Tegalrejo, Ringinkembar, Sekarbanyu, Klepu, Sumbermanjing Wetan, and Sitiarjo frequently form clusters of extreme vulnerability. Sidoasri, Tambaksari, and Kedungbanteng are in the lowest risk category. These differing spatial patterns indicate there is no consistent hazard gradient. Significant local differences in hazard intensity, socioeconomic exposure, and institutional capacity shape the final risk pattern [36].

Extreme physical hazards alone do not determine high-risk labels. A specific combination drives vulnerability at the village level: medium hazard exposure, severe vulnerability, and limited capacity. Tegalrejo and Argotirto serve as good examples of this mechanism. Their closeness to rivers results in regular flooding. However, poor institutional readiness, limited healthcare access, and high population density push these villages into the high-risk category [36]. In contrast, low-risk areas have the opposite structural setup. Hazard exposure is lower. Capacity is moderate. Access to basic services has slight improvements. Therefore, hazard

layers alone cannot indicate absolute risk. The actual risk pattern comes from the mathematical intersection of all three measures [44].

Global rural topologies show the same spatial patterns. Structural capacity shortcomings often overshadow the severity of physical hazards. Assessments of the Algerian Cheliff-Ghrib watershed used AHP to classify 22% of regional areas as extreme risk. Infrastructural issues and social conditions heavily influenced this result. The impact of physical hazard metrics was minimal [45]. Vietnamese spatial modeling, which combined deep learning and MCDA techniques, revealed similar findings. Institutional capacity gaps played a key role in shaping the distribution of risk [46]. Urban spatial models support these conclusions from rural areas. Frameworks from Toronto demonstrated that adding socioeconomic indicators significantly improves spatial predictive accuracy compared to relying solely on physical hazard mapping [47]. These international spatial observations closely reflect the outputs from the Sumbermanjing Wetan region.

Extreme spatial clustering defines the high-risk outputs. Argotirto, Harjokuncaran, Tegalrejo, and Ringinkembar form a contiguous northern vulnerability corridor. Moderate physical hazard, extreme socioeconomic vulnerability, and minimal institutional capacity intersect exactly within these administrative boundaries. This strict geographic concentration optimizes disaster planning operations. Targeted spatial interventions within this specific northern sector maximize demographic protection. Localized mitigation strategies eliminate inefficient district-wide resource distributions lacking empirical spatial priority.

Equation 3 mathematically dictates this specific spatial output. District-wide physical hazard values remain statistically low. Numerous administrative units still register severe final risk scores. Socioeconomic vulnerability has a significantly broader spatial footprint than raw physical hazard. It consistently records higher absolute index values. This parameter serves as the dominant mathematical driver in the risk formulation. Capacity metrics operate inversely. Minor capacity reductions trigger massive spikes in the composite risk score. Severe healthcare deficits and minimal preparedness data prove this mathematical sensitivity. Moderate hazard environments generate extreme risk classifications strictly due to systemic local response failures. The risk algorithm exhibits extreme mathematical sensitivity to fluctuations in vulnerability and capacity. These human-driven parameters completely override absolute physical hazard shifts.

Conventional urban flood models demonstrate fundamentally different risk mechanisms. Hazard intensity typically dictates urban spatial risk. Rural topologies like Sumbermanjing Wetan completely reject this baseline assumption. Institutional constraints and absolute socioeconomic conditions dictate the distribution of primary risks. Actual inundation events frequently materialize within classified low-hazard boundaries. Strict parameter generalization completely fails to capture these localized anomalies. Average precipitation metrics and broad land system classifications mask critical micro-variables. Small-scale hydrological fluctuations, localized drainage failures, and episodic extreme precipitation remain structurally unrecorded [48]. The current multi-criteria index provides robust macro-scale regional screening. Operational utility at the regional level remains extremely high. Conversely, this identical spatial generalization guarantees severe analytical blind spots at micro-spatial resolutions.

Theoretical frameworks dictate strict nonlinear interactions among parameters. Absolute flood risk operates exclusively as a multi-dimensional product of hazard, vulnerability, and capacity. Isolated physical hazard functions fundamentally fail to model spatial risk. Index-based geospatial models inherently lack the mathematical precision of machine learning algorithms or physically based hydrodynamic simulations. They cannot calculate specific inundation velocity, absolute depth, or temporal propagation dynamics. The methodology inherently enforces rigid spatial generalizations. Regardless, data-scarce environments strictly demand these simplified operational models. They delineate priority mitigation zones efficiently. The framework completely bypasses the requirement for advanced computational infrastructure or unavailable high-resolution environmental inputs. Subsequent spatial research must explicitly couple these composite indices with physical hydrodynamic simulations. This methodological integration maximizes spatial predictive accuracy while preserving operational feasibility [49].

The spatial results strictly dictate two operational pathways. Local governments must use these map outputs to target resource allocation. Uniform disaster fund distribution guarantees critical resource exhaustion. Pure physical hazard mitigation inherently fails. Absolute socioeconomic vulnerability dictates the actual spatial risk. Regional authorities must aggressively upgrade medical infrastructure, telecommunication networks, and institutional readiness strictly within the northern vulnerability corridor. Ecosystem-based spatial adaptations require immediate deployment. Coastal mangrove systems physically dissipate incoming wave energy. Riparian vegetation mechanically stabilizes active riverbanks and absorbs channel overflow. Upstream reforestation drastically cuts peak watershed discharge [50]. Methodological constraints demand

immediate subsequent attention. The absence of hydrodynamic validation and empirical flood-depth calibration severely limits the precision of the final index [51,52]. Future spatial research must execute ensemble modeling alongside physically based hydrological simulations [36,46]. These advanced computational techniques will expand directly upon the baseline spatial prioritization established within this framework.

Transportation and communication networks exhibit extreme spatial asymmetry. All local road networks maintain paved surfaces ensuring year-round access. Conversely, fixed public transport routes entirely bypass multiple administrative zones. Rural populations strictly depend on irregular transit modes. Communication infrastructure demonstrates severe maldistribution. Thirty-two base transceiver stations serve only 15 villages. Harjokuncaran operates seven towers. Tegalrejo possesses zero [36]. This specific communication void completely paralyses inter-village coordination during severe inundation events. Emergency response times degrade exponentially. Extreme flood events in Thailand exposed identical infrastructural constraints [40]. Absolute resource quantities fail to guarantee community resilience. Effective mitigation strictly requires precise spatial distribution.

International spatial literature corroborates this specific mechanism. Dutch case studies show that knowledge-sharing networks and active community participation significantly enhance disaster preparedness. Physical infrastructure alone fundamentally fails to replicate these social buffers [41]. South Korean disaster analysis confirms this operational dynamic. Local institutional strength and organizational redundancy strictly separate resilient from vulnerable urban sectors [42]. Furthermore, physical drainage and transport networks must conform strictly to actual local topography. Statistical benchmarks provide zero operational value during actual inundation [43]. Sumbermanjing Wetan fails all these structural preconditions. Medical services completely lack functional redundancy. Educational access vanishes at district perimeters. Public transport coverage remains heavily fragmented. Spatial blind spots dominate the local communication grid. Immediate capacity-building interventions must aggressively redistribute existing services and upgrade peripheral infrastructure.

Absolute agricultural dependency severely amplifies spatial vulnerability. The entire district contains only 11 permanent or semi-permanent market facilities. *Capsicum frutescens* and *Capsicum annuum* (chili) cultivation strictly dominated the 2023 agricultural output. Monoculture economies collapse rapidly under acute disaster stress. Inundation physically destroys standing crops and severs critical distribution logistics. Without alternative economic streams, post-disaster recovery stagnates. Previous empirical literature documents identical mechanisms in rural Nepal. Subsistence agriculture and absolute capacity constraints directly dictated household-level vulnerability [37]. Systematic geospatial reviews corroborate this exact multifactorial dynamic. Social, economic, and environmental parameters function strictly as interdependent networks, never operating in isolation [38].

Asian rural areas often exhibit similar structural problems: poor infrastructure, limited institutional support, and a lack of economic diversity [39]. Sumbermanjing Wetan is a clear example of this vulnerability. Overcrowded communities strained medical resources, and a heavy reliance on agriculture contribute to a high vulnerability rate of 28.24%. To reduce disaster risks, immediate structural changes are necessary. Local authorities need to actively increase the medical workforce and improve health centers. At the same time, policymakers should create different economic options that are not tied to seasonal monoculture practices [36,37]. Field documentation of these flood impacts in Sumbermanjing Wetan is presented in Figure 5.

(a) **(b)** **(c)**

Figure 5. Field documentation of flood events in Sumbermanjing Wetan District. (a) shows surface flooding entering residential areas. (b) shows local housing being submerged. (c) shows emergency personnel carrying out evacuation efforts. Source: AntaraNews.

Conclusion

Socioeconomic deficits and institutional constraints dictate regional flood risk far beyond absolute physical hazard metrics. Low-hazard spatial coverage dominates the district. Severe risk clusters persistently within specific administrative boundaries. Extreme demographic exposure, rigid agricultural dependency, and minimal institutional preparedness strictly drive this spatial outcome. These human-driven variables drastically inflate systemic vulnerability. They simultaneously suppress local adaptive capacity. Favorable topographical parameters completely fail to offset these structural deficits. In rural settings, the socioeconomic structure and the uneven geography of services shape risk outcomes more decisively than hazard indicators do — and the spatial pattern here bears that out. For village-level planning, this means that resource prioritization cannot be based solely on the hazard map. Healthcare access, communication, and transport reach, and institutional preparedness in high-vulnerability, low-capacity villages are where risk reduction has the most leverage. Mangrove conservation along the coast, riparian vegetation management along river channels, and upstream watershed restoration work in the same direction, addressing the physical side of exposure without displacing the socioeconomic investments that the data point to more urgently. However, this study also reveals that the index-based approach may not fully capture localized flood dynamics, as indicated by flood events occurring in areas classified as low hazard. The reliance on generalized parameters such as average rainfall and land system data may lead to an underestimation of hazard and risk at finer spatial scales. Therefore, while the model remains useful for regional-scale screening in data-limited contexts, future research should integrate higher-resolution spatial data, remote-sensing-based flood observations, and physically based hydrological or hydrodynamic models to improve accuracy and better represent local flood processes.

Author Contributions

LYI: Conceptualization, Methodology, Software, Investigation, Writing - Review & Editing; **MNH**: Writing - Review & Editing, Software, Investigation; **IHP**: Writing - Review & Editing, Software, Investigation and **MTM**: Writing - Review & Editing, Supervision.

AI Writing Statement

During the preparation of this work, the authors used generative AI tools for language editing and manuscript refinement. After using these tools, the authors carefully reviewed and revised the content and take full responsibility for the final manuscript.

Conflicts of interest

There are no conflicts to declare.

Acknowledgments

The authors want to appreciate LPPM UM for providing funding for this research activity. Thank you also to the DRRE research team, who have assisted in carrying out research activities.

References

1. Cea, L.; Costabile, P. Flood Risk in Urban Areas: Modelling, Management and Adaptation to Climate Change. A Review. *Hydrology* **2022**, *9*, 50, doi:10.3390/hydrology9030050
2. Alfieri, L.; Bisselink, B.; Dottori, F.; Naumann, G.; de Roo, A.; Salamon, P.; Wyser, K.; Feyen, L. Global Projections of River Flood Risk in a Warmer World. *Earth's Future* **2017**, *5*, 171–182, doi:10.1002/2016EF000485
3. Nguyen, H.D.; Nguyen, T.H.T.; Nguyen, Q.H.; Nguyen, T.G.; Dang, D.K.; Nguyen, Y.N.; Bui, T.H.; Nguyen, N.D.; Bui, Q.T.; Brecan, P.; Petrisor, A.I. Bottom-up Approach for Flood-Risk Management in Developing Countries: A Case Study in the Gianh River Watershed of Vietnam. *Nat. Hazards* **2023**, *118* (3), 1933–1959, doi:10.1007/s11069-023-06098-4.

4. Ziwei, L.; Xiangling, T.; Liju, L.; Yanqi, C.; Xingming, W.; Dishan, Y. GIS-Based Risk Assessment of Flood Disaster in the Lijiang River Basin. *Sci. Rep.* **2023**, *13* (1), 1–13, doi:10.1038/s41598-023-32829-5.
5. Baggio, T.; Martini, M.; Bettella, F.; D'Agostino, V. Debris Flow and Debris Flood Hazard Assessment in Mountain Catchments. *Catena* **2024**, *245*, doi:10.1016/j.catena.2024.108338.
6. Paprotny, D.; Sebastian, A.; Morales-Nápoles, O.; Jonkman, S.N. Trends in Flood Losses in Europe over the Past 150 Years. *Nat. Commun.* **2018**, *9* (1), doi:10.1038/s41467-018-04253-1.
7. Jongman, B.; Ward, P.J.; Aerts, J.C.J.H. Global Exposure to River and Coastal Flooding: Long Term Trends and Changes. *Glob. Environ. Change* **2012**, *22*, 823–835, doi:10.1016/j.gloenvcha.2012.07.004.
8. Tanoue, M.; Hirabayashi, Y.; Ikeuchi, H. Global-Scale River Flood Vulnerability in the Last 50 Years. *Sci. Rep.* **2016**, *6*, 1–9, doi:10.1038/srep36021.
9. Ward, P.J.; Jongman, B.; Aerts, J.C.J.H.; Bates, P.D.; Botzen, W.J.W.; Loaiza, A.D.; Hallegatte, S.; Kind, J. M.; Kwadijk, J.; Scussolini, P.; Winsemius, H. C. A Global Framework for Future Costs and Benefits of River-Flood Protection in Urban Areas. *Nat. Clim. Chang.* **2017**, *7* (9), 642–646, doi:10.1038/nclimate3350.
10. Stanton-Geddes, Z.; Vun, Y.J. Strengthening the Disaster Resilience of Indonesian Cities. In *Time to ACT: Realizing Indonesia's Urban Potential*; World Bank: Washington, DC, USA, 2019;
11. Varra, G.; Della Morte, R.; Tartaglia, M.; Fiduccia, A.; Zammuto, A.; Agostino, I.; Booth, C.A.; Quinn, N.; Lamond, J.E.; Cozzolino, L. Flood Susceptibility Assessment for Improving the Resilience Capacity of Railway Infrastructure Networks. *Water (Switzerland)* **2024**, *16* (18), doi:10.3390/w16182592
12. Güneralp, B.; Güneralp, İ.; Liu, Y. Changing Global Patterns of Urban Exposure to Flood and Drought Hazards. *Glob. Environ. Chang.* **2015**, *31*, 217–225, doi:10.1016/j.gloenvcha.2015.01.002.
13. Tanim, A.H.; McRae, C.B.; Tavakol-Davani, H.; Goharian, E. Flood Detection in Urban Areas Using Satellite Imagery and Machine Learning. *Water* **2022**, *14* (7), 1140, doi:10.3390/w14071140.
14. Dharmarathne, G.; Waduge, A.O.; Bogahawaththa, M.; Rathnayake, U.; Meddage, D.P.P. Adapting Cities to the Surge: A Comprehensive Review of Climate-Induced Urban Flooding. *Results Eng.* **2024**, *22*, 102123, doi:10.1016/j.rineng.2024.102123.
15. Papathoma-Köhle, M. Vulnerability Curves vs. Vulnerability Indicators: Application of an Indicator-Based Methodology for Debris-Flow Hazards. *Nat. Hazards Earth Syst. Sci.* **2016**, *16* (8), 1771–1790, doi:10.5194/nhess-16-1771-2016.
16. Lendering, K.T.; Jonkman, S.N.; Kok, M. Effectiveness of Emergency Measures for Flood Prevention. *J. Flood Risk Manag.* **2016**, *9* (4), 320–334, doi:10.1111/jfr3.12185.
17. Chan, S.W.; Abid, S.K.; Sulaiman, N.; Nazir, U.; Azam, K. A Systematic Review of the Flood Vulnerability Using Geographic Information System. *Heliyon* **2022**, *8* (3), e09075, doi:10.1016/j.heliyon.2022.e09075.
18. Diriba, D.; Takele, T.; Karuppannan, S.; Husein, M. Flood Hazard Analysis and Risk Assessment Using Remote Sensing, GIS, and AHP Techniques: A Case Study of the Gidabo Watershed, Main Ethiopian Rift, Ethiopia. *Geomatics, Nat. Hazards Risk* **2024**, *15* (1), doi:10.1080/19475705.2024.2361813.
19. Ariyani, D.; Purwanto, M.Y.J.; Sunarti, E.; Perdinan, P.; Juniati, A.T. Integrated Flood Hazard Assessment Using Multi-Criteria Analysis and Geospatial Modeling. *J. Degrad. Min. Lands Manag.* **2024**, *11* (4), 6121–6134, doi:10.15243/jdmlm.2024.114.6121.
20. Domeneghetti, A.; Carisi, F.; Castellarin, A.; Brath, A. Evolution of Flood Risk over Large Areas: Quantitative Assessment for the Po River. *J. Hydrol.* **2015**, *527*, 809–823, doi:10.1016/j.jhydrol.2015.05.043.
21. Pakati, S.S.; Shoko, C.; Dube, T. Integrated Flood Modelling and Risk Assessment in Urban Areas: A Review on Applications, Strengths, Limitations and Future Research Directions. *J. Hydrol. Reg. Stud.* **2025**, *61*, 102583, doi: 10.1016/j.ejrh.2025.102583.
22. Lawrence, D. Uncertainty Introduced by Flood Frequency Analysis in Projections for Changes in Flood Magnitudes under a Future Climate in Norway. *J. Hydrol. Reg. Stud.* **2020**, *28*, 100675, doi:10.1016/j.ejrh.2020.100675.
23. Supratman, M.; Kusuma, M.S.B.; Cahyono, M.; Kuntoro, A.A. Flood Hazard Assessment Due to Changes in Land Use and Cover. *Civ. Eng. J.* **2024**, *10* (12), 3874–3891, doi:10.28991/CEJ-2024-010-12-04.

24. Mukherjee, J.; Chowdhury, A.; Ghosh, S. Enhancing Watershed Management Through Advanced Geospatial and Morphometric Approaches for Wainganga River Basin, Central India; 2025; pp 563–598, doi:10.1007/978-3-031-62376-9_25.
25. Alawiyah, A. M.; Harintaka, H. Identifikasi Genangan Banjir Di Wilayah DKI Jakarta Menggunakan Citra Satelit Sentinel-1. *JGISE J. Geospatial Inf. Sci. Eng.* **2021**, *4* (2), 95, doi:10.22146/jgise.68353.
26. Arianti, I.; Rafani, M.; Wattini; Fitriani, N.; Nizar; Vatria, B. Development of an Adaptive Drainage System for Flood Mitigation Using GIS. *Eur. J. Appl. Sci. Eng. Technol.* **2024**, *2* (6), 81–89, doi:10.59324/ejaset.2024.2(6).07.
27. Handayani, W.; Fisher, M.R.; Rudiarto, I.; Sih Setyono, J.; Foley, D. Operationalizing Resilience: A Content Analysis of Flood Disaster Planning in Two Coastal Cities in Central Java, Indonesia. *Int. J. Disaster Risk Reduct.* **2019**, *35*, 101073, doi:10.1016/j.ijdrr.2019.101073.
28. Badan Nasional Penanggulangan Bencana (BNPB). *Peraturan Kepala Badan Nasional Penanggulangan Bencana Nomor 02 Tahun 2012 tentang Pedoman Umum Pengkajian Risiko Bencana.* BNPB: Jakarta, Indonesia, 2012.
29. Ahmed, N.; Hoque, M. A.-A.; Howlader, N.; Pradhan, B. Flood Risk Assessment: Role of Mitigation Capacity in Spatial Flood Risk Mapping. *Geocarto Int.* **2022**, *37* (25), 8394–8416, doi:10.1080/10106049.2021.2002422
30. Khoeun, C.; Sok, T.; Chan, R.; Khe, S.; Ich, I.; Chan, K.; Oeurng, C. Assessing Flood Hazard Index Using Analytical Hierarchy Process (AHP) and Geographical Information System (GIS) in Stung Sen River Basin. *IOP Conf. Ser. Earth Environ. Sci.* **2022**, *1091* (1, doi:10.1088/1755-1315/1091/1/012031.
31. Baky, M.A.A.; Islam, M.; Paul, S. Flood Hazard, Vulnerability and Risk Assessment for Different Land Use Classes Using a Flow Model. *Earth Syst. Environ.* **2020**, *4* (1), 225–244, doi:10.1007/s41748-019-00141-w.
32. Ouma, Y.O.; Tateishi, R. Urban Flood Vulnerability and Risk Mapping Using Integrated Multi-Parametric AHP and GIS: Methodological Overview and Case Study Assessment. *Water (Switzerland)* **2014**, *6* (6), 1515–1545, doi:10.3390/w6061515
33. Kelman, I.; Glantz, M.H. Analyzing the Sendai Framework for Disaster Risk Reduction. *Int. J. Disaster Risk Sci.* **2015**, *6* (2), 105–106, doi:10.1007/s13753-015-0056-3.
34. Luu, C.; Von Meding, J.; Kanjanabootra, S. Assessing Flood Hazard Using Flood Marks and Analytic Hierarchy Process Approach: A Case Study for the 2013 Flood Event in Quang Nam, Vietnam. *Nat. Hazards* **2018**, *90* (3), 1031–1050, doi:10.1007/s11069-017-3083-0.
35. Dung, N.B.; Long, N.Q.; Goyal, R.; An, D.T.; Minh, D.T. The Role of Factors Affecting Flood Hazard Zoning Using Analytical Hierarchy Process: A Review. *Earth Syst. Environ.* **2022**, *6* (3), 697–713, doi:10.1007/s41748-021-00235-4.
36. Badan Pusat Statistik (BPS) Kabupaten Malang. Kecamatan Sumbermanjing Wetan Dalam Angka 2024. BPS Kabupaten Malang: Malang, Indonesia, 2024;
37. Pathak, S.; Panta, H.K.; Bhandari, T.; Paudel, K.P. Flood Vulnerability and Its Influencing Factors. *Nat. Hazards* **2020**, *104* (3), 2175–2196, doi:10.1007/s11069-020-04267-3.
38. Rehman, S.; Sahana, M.; Hong, H.; Sajjad, H.; Ahmed, B. A Systematic Review on Approaches and Methods Used for Flood Vulnerability Assessment: Framework for Future Research. *Nat. Hazards* **2019**, *96* (2), 975–998, doi:10.1007/s11069-018-03567-z.
39. Nasiri, H.; Yusof, M.J.M.; Ali, T.A.M. An Overview to Flood Vulnerability Assessment Methods. *Sustain. Water Resour. Manag.* **2016**, *2* (3), 331–336, doi:10.1007/s40899-016-0051-x.
40. Thanvisitthpon, N.; Shrestha, S.; Pal, I.; Ninsawat, S.; Chaowiwat, W. Assessment of Flood Adaptive Capacity of Urban Areas in Thailand. *Environ. Impact Assess. Rev.* **2020**, *81* (May 2019), 106363, doi:10.1016/j.eiar.2019.106363.
41. de Voogt, D.L.; Bisschops, S.; Munaretto, S. Participatory Social Capacity Building: Conceptualisation and Experiences from Pilots for Flood Risk Mitigation in the Netherlands. *Environ. Sci. Policy* **2019**, *99*, 89–96, doi:10.1016/j.envsci.2019.05.019.

42. Ro, B.; Garfin, G. Building Urban Flood Resilience through Institutional Adaptive Capacity: A Case Study of Seoul, South Korea. *Int. J. Disaster Risk Reduct.* **2023**, *85* (August 2022), 103474, doi:10.1016/j.ijdrr.2022.103474.
43. Singh, A.; Dawson, D.; Trigg, M.A.; Wright, N.; Seymour, C.; Ferriday, L. Drainage Representation in Flood Models: Application and Analysis of Capacity Assessment Framework. *J. Hydrol.* **2023**, *622* (PA), 129718, doi:10.1016/j.jhydrol.2023.129718.
44. Saber, M.; Boulmaiz, T.; Guermoui, M.; Abdrabo, K.I.; Kantoush, S.A.; Sumi, T.; Boutaghane, H.; Hori, T.; van Binh, D.; Nguyen, B.Q.; Bui, T.T.P.; Vo, N.D.; Habib, E.; Mabrouk, E. Enhancing Flood Risk Assessment through Integration of Ensemble Learning Approaches and Physical-Based Hydrological Modeling. *Geomatics, Nat. Hazards Risk* **2023**, *14* (1), doi:10.1080/19475705.2023.2203798.
45. Mokhtari, E.; Mezali, F.; Abdelkebir, B.; Engel, B. Flood Risk Assessment Using Analytical Hierarchy Process: A Case Study from the Cheliff-Ghrib Watershed, Algeria. *J. Water Clim. Chang.* **2023**, *14* (3), 694–711, doi:10.2166/wcc.2023.316.
46. Pham, B. T.; Luu, C.; van Dao, D.; van Phong, T.; Nguyen, H. D.; van Le, H.; von Meding, J.; Prakash, I. Flood Risk Assessment Using Deep Learning Integrated with Multi-Criteria Decision Analysis. *Knowledge-Based Syst.* **2021**, *219*, 106899, doi:10.1016/j.knosys.2021.106899.
47. Rincón, D.; Khan, U. T.; Armenakis, C. Flood Risk Mapping Using GIS and Multi-Criteria Analysis: A Greater Toronto Area Case Study. *Geosciences* **2018**, *8* (8), 275, doi:10.3390/geosciences8080275.
48. Taoukidou, N.; Karpouzos, D.; Georgiou, P. Flood Hazard Assessment Through AHP, Fuzzy AHP, and Frequency Ratio Methods: A Comparative Analysis. *Water (Switzerland)* **2025**, *17*, doi: 10.3390/w17142155.
49. Khan, N.A.; Alzahrani, H.; Bai, S.; Hussain, M.; Tayyab, M.; Ullah, S.; Ullah, K.; Khalid, S. Flood Risk Assessment in the Swat River Catchment through GIS-Based Multi-Criteria Decision Analysis. *Front. Environ. Sci.* **2025**, *13*, 1–18, doi: 10.3389/fenvs.2025.1567796.
50. OECD. Nature-Based Solutions for Flood Management in Asia and the Pacific. Available online: www.oecd.org/dev/wp.%0Ahttps://www.oecd-ilibrary.org/development/nature-based-solutions-for-flood-management-in-asia-and-the-pacific_f4c7bcbe-en (accessed on 3 June 2025)
51. Filho, W.L.; Alam, G.M.M.; Nagy, G.J.; Rahman, M.M.; Roy, S.; Wolf, F.; Kovaleva, M.; Saroar, M.; Li, C. Climate Change Adaptation Responses among Riparian Settlements: A Case Study from Bangladesh. *PLoS One* **2022**, *17*, 1–19, 2022, doi: 10.1371/journal.pone.0278605.
52. Irawan, L.Y.; Sumarmi, Panoto, D.; Pradana, I.H.; Faizal, R.; Devy, M.M.R.; Putra, D.B.P. The Identification of Flood Susceptibility and Its Contributing Factors in Sampang Regency. *IOP Conf. Ser. Earth Environ. Sci.* **2022**, *1089*, doi: 10.1088/1755-1315/1089/1/012013.